JCTC Journal of Chemical Theory and Computation

Article

pubs.acs.org/JCTC

Efficient Calculations of Molecular Linear Response Properties for Spectral Regions

Joanna Kauczor* and Patrick Norman*

Department of Physics, Chemistry and Biology, Linköping University, SE-581 83 Linköping, Sweden

ABSTRACT: Molecular spectra can be determined from molecular response functions, by solving the so-called damped response equations using the complex polarization propagator approach. The overall structure of response equations is identical for variational wave functions such as the Hartree−Fock, multiconfiguration self-consistent field, and Kohn−Sham density functional theory, and the key program module is the linear response equation solver. We present an implementation of the solver using the algorithm with symmetrized vectors, optimized for addressing spectral regions of a width of some 5−10 eV and a resolution below 0.1 eV. The work is illustrated by the consideration of UV−vis as well as near carbon *K* -edge absorption spectra of the C_{60} fullerene. We demonstrate that it is possible to converge tightly response equations for hundreds of optical frequencies in resonance regions of the spectrum at a cost not much exceeding the solution of a single response equation in the nonresonant region. Our work is implemented in the molecular orbital based module of the Dalton program and serves as a documentation of the code distributed in the Dalton2013 release version.

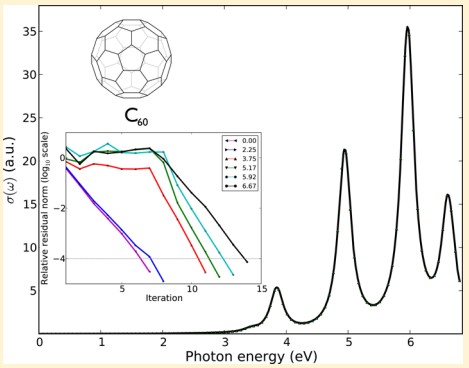

I. INTRODUCTION

Molecular properties for ground and excited states as well as for transitions between these states can be determined from molecular response functions.[1] In formulations of conventional response theory, transition energies and strengths are obtained from poles and residues of response functions, respectively, and spectroscopic properties are therefore obtained by solving a generalized eigenvalue problem. The iterative procedures that are adopted to solve this eigenvalue equation provide excitation energies starting from the lowest excited states (so-called *bottom-up* approaches), which is a technique that makes it prohibitively difficult to address spectral regions with high density-of-states (DOS). Situations of high DOS will inevitably be of concern in studies of large and complex systems or inner-shell spectroscopies. In matrix algebra, a remedy to the described problem is provided by any number of variants of the Lanczos algorithm,[2] a path followed also by us in the coupled cluster framework.[3] In applied work, however, a Lanczos-based implementation of response theory comes with its share of drawbacks, most notably a lack of error control and an inherently serial nature in the algorithm. These aspects have proven prohibitive in X-ray absorption spectroscopies, where chain lengths of 10^4−10^5 are needed to obtain adequate convergence of response equations.[4]

An alternative solution to the problem of high DOS in molecular response theory is provided by the complex polarization propagator approach (CPP).[5,6] In CPP, a damping term γ is introduced, denoting the inverse excited state lifetime and taking relaxation into account.[5−13] From a purely computational perspective, it amounts to introducing complex excitation energies that removes singularities of the response functions at resonance frequencies. Such a modification leads to real and imaginary components of response functions that are connected by Kramers−Kronig relations and describing scattering and absorption phenomena. Damped response theory can be applied to any frequency region of interest and provides spectroscopic properties with full error control. It has been successfully applied to a wide range of molecular properties including UV−vis absorption and dispersion coefficients,[5,10,14−19] optical rotation and electronic circular dichroism,[20−22] X-ray absorption and natural circular dichroism spectra,[23−27] dynamic dipole magnetizability,[28] Raman scattering,[29−35] electro-optical Kerr effect, magnetic circular dichroism spectra,[36−39] and two-photon resonant enhanced second-harmonic generation.[6,40,41]

The overall structure of response equations is identical for variational wave functions such as the Hartree−Fock (HF), multiconfiguration self-consistent field (MCSCF), and Kohn−Sham density functional theory (KS-DFT), and the key program module is the linear response equation solver. The large dimensionality of the involved matrices imposes the use of iterative algorithms, and criteria against which such solver routines are evaluated are stability and efficiency. The traditional way of solving large sets of linear equations is based on the iterative subspace approaches. In ref 42, Olsen et al. introduced paired trial vectors in the iterative subspace algorithm, which highly improved the performance of the Davidson algorithm[43] used for solving the eigenvalue response equation and improvement in convergence of the standard response equation was also observed. This approach was adopted by Norman et al.[5,6] and Kristensen et al.[10] in algorithms proposed for solving damped response equations. Saue and co-workers[44−46] introduced a symmetry division of trial vectors for solving response equations

Received: February 12, 2014
Published: May 12, 2014

in the four-component HF and DFT approximations. In their approach, trial vectors are split according to their hermiticity and time-reversal symmetry, which are the two fundamental operator symmetries in a relativistic framework. This, in turn, led to the development of a symmetrized trial vectors algorithm in the nonrelativistic realm that proved highly stable for the solution of the complex linear response equation,[11] as demonstrated in nanoparticle applications.[19,27,39] Recently, it has been combined with the polarizable embedding scheme,[47] so that resonance spectroscopies of large and complex systems can be addressed. We have also introduced an analogous iterative subspace algorithm for solving damped response equations at the coupled cluster level of theory.[48]

The goal of the present paper is to turn the stable algorithm presented in ref 11 into an efficient algorithm and program implementation, optimized for addressing spectral regions of a width of some 5−10 eV and a resolution below 0.1 eV. The spectroscopy at hand determines the placement of this window of spectral frequencies, as illustrated in the present work by the consideration of UV−vis as well as near carbon K -edge absorption spectra of the C_{60} fullerene. We will demonstrate that it is possible to converge tightly response equations for hundreds of optical frequencies in resonance regions of the spectrum at a cost not much exceeding the solution of a single response equation in the nonresonant region. Our work is implemented in the molecular orbital (MO) based module of the Dalton program and serves as a documentation of the code distributed in the Dalton2013 release version.[49] The algorithm as such, however, is not limited to an MO formulation of response theory, and it will also be implemented in the atomic-orbital driven part of Dalton (LSDalton) that displays linear scaling characteristics.

II. THEORY

The cross-section for linear absorption of radiation by a randomly oriented molecular sample can, in electric-dipole approximation, be expressed as

$$\sigma(\omega) = \frac{4\pi\omega}{c}\mathrm{Im}\,\bar{\alpha}(\omega) \tag{1}$$

$\bar{\alpha}(\omega)$ denotes the isotropic average dipole polarizability at frequency ω and is defined as

$$\bar{\alpha} = \frac{1}{3}(\alpha_{xx} + \alpha_{yy} + \alpha_{zz}) \tag{2}$$

The polarizability corresponds to the first-order response in the molecular dipole moment to an external electric field.

For a general optical frequency, ω, the dipole polarizability may be expressed in terms of a sum-overstates formula as

$$\alpha_{\alpha\beta}(\bar{\omega}) = \frac{1}{\hbar}\sum_{n>0}\left[\frac{\langle 0|\hat{\mu}_\alpha|n\rangle\langle n|\hat{\mu}_\beta|0\rangle}{\omega_{0n} - \omega} + \frac{\langle 0|\hat{\mu}_\beta|n\rangle\langle n|\hat{\mu}_\alpha|0\rangle}{\omega_{0n} + \omega}\right] \tag{3}$$

where $\hat{\mu}_\alpha$ refers to the electric dipole operator along the molecular axis α and $\hbar\omega_{0n}$ is the transition energy between the ground and excited state, $|0\rangle \rightarrow |n\rangle$. Equation 3 diverges when the frequency ω of the external field approaches any of the transition frequencies ω_{0n} of the system. Damping terms (so-called finite lifetimes parameters) can be introduced in the linear response function[5,6] that correspond to line-broadenings in the absorption spectra, thereby yielding the *damped* linear response function. By adopting a common damping parameter γ for all excited states, the dipole polarizability may be expressed as

$$\alpha_{\alpha\beta}(\omega) = \frac{1}{\hbar}\sum_{n>0}\left[\frac{\langle 0|\hat{\mu}_\alpha|n\rangle\langle n|\hat{\mu}_\beta|0\rangle}{\omega_{0n} - (\omega + i\gamma)} + \frac{\langle 0|\hat{\mu}_\beta|n\rangle\langle n|\hat{\mu}_\alpha|0\rangle}{\omega_{0n} + (\omega + i\gamma)}\right] \tag{4}$$

where the imaginary term $i\gamma$ is associated with the external frequency ω, rather than the transition frequency ω_{0n}. Thus, damped linear response theory effectively corresponds to introducing a complex optical frequency $\omega \rightarrow \omega + i\gamma$, which implies solving response equations with complex frequencies.[5,6,10]

It has previously been shown that eq 4 can be evaluated at any general complex-frequency argument using the complex polarization propagator approach,[5,6] where $\alpha_{\alpha\beta}(\omega)$ can be identified from the complex (damped) linear response functions. In the single determinant HF or KS-DFT approximations, the polarizability in eq 4 corresponds to[1,5]

$$\langle\langle A; B\rangle\rangle_\omega = -\mathbf{A}^{[1]\dagger}\{\mathbf{E}^{[2]} - (\omega^R + i\omega^I)\mathbf{S}^{[2]}\}^{-1}\mathbf{B}^{[1]} \tag{5}$$

where $\mathbf{E}^{[2]}$ and $\mathbf{S}^{[2]}$ are the Hessian and metric matrices, respectively, and $\mathbf{A}^{[1]}$ and $\mathbf{B}^{[1]}$ denote property gradients corresponding to the components of the polarizability. The polarizability in eq 5 can be obtained by solving the complex response equations

$$[\mathbf{E}^{[2]} - (\omega + i\gamma)\mathbf{S}^{[2]}](\mathbf{X}^R + i\mathbf{X}^I) = \mathbf{G}^R + i\mathbf{G}^I \tag{6}$$

using the algorithm with symmetrized trial vectors introduced in ref 11, and described in details in the next section.

III. ALGORITHM

The algorithm with symmetrized trial vectors is an iterative subspace procedure that combines fast convergence with a very efficient scheme for obtaining new trial vectors. It relies on expressing the trial vector as the sum of real (R) and imaginary (I), symmetric (g) and antisymmetric (u) components

$$\mathbf{x} = \mathbf{x}_g^R + \mathbf{x}_u^R + i(\mathbf{x}_u^I + \mathbf{x}_g^I) \tag{7}$$

where $\mathbf{x}_g^R$, $\mathbf{x}_u^R$, $\mathbf{x}_g^I$, and $\mathbf{x}_u^I$ are real. It also exploits the features of the linear transformations $\mathbf{E}^{[2]}$ and $\mathbf{S}^{[2]}$ on a vector. The symmetry of a vector is conserved (reversed) for the $\mathbf{E}^{[2]}$ ($\mathbf{S}^{[2]}$) linear transformation

$$\boldsymbol{\sigma}_g = \mathbf{E}^{[2]}\mathbf{b}_g; \quad \boldsymbol{\sigma}_u = \mathbf{E}^{[2]}\mathbf{b}_u \tag{8a}$$

$$\boldsymbol{\rho}_g = \mathbf{S}^{[2]}\mathbf{b}_u; \quad \boldsymbol{\rho}_u = \mathbf{S}^{[2]}\mathbf{b}_g \tag{8b}$$

that makes it advantageous to split the solution to the damped response equations (eq 6) into symmetric and antisymmetric components. Using this method, the paired structure of the Hessian and metric matrices is imposed in the reduced space during the whole iterative procedure and effects in improving the convergence speed.[42]

Inserting eq 7 into the damped response equation in eq 6 gives a set of linear equations for each of the four components $\mathbf{X}_g^R$, $\mathbf{X}_u^R$, $\mathbf{X}_g^I$, and $\mathbf{X}_u^I$

$$\begin{aligned}
\mathbf{E}^{[2]}\mathbf{X}_g^R - \omega\mathbf{S}^{[2]}\mathbf{X}_u^R + \gamma\mathbf{S}^{[2]}\mathbf{X}_u^I &= \mathbf{G}_g^R \\
\mathbf{E}^{[2]}\mathbf{X}_u^R - \omega\mathbf{S}^{[2]}\mathbf{X}_g^R + \gamma\mathbf{S}^{[2]}\mathbf{X}_g^I &= \mathbf{G}_u^R \\
\mathbf{E}^{[2]}\mathbf{X}_u^I - \omega\mathbf{S}^{[2]}\mathbf{X}_g^I - \gamma\mathbf{S}^{[2]}\mathbf{X}_g^R &= \mathbf{G}_u^I \\
\mathbf{E}^{[2]}\mathbf{X}_g^I - \omega\mathbf{S}^{[2]}\mathbf{X}_u^I - \gamma\mathbf{S}^{[2]}\mathbf{X}_u^R &= \mathbf{G}_g^I
\end{aligned} \tag{9}$$

where $\mathbf{G}_g^R$ and $\mathbf{G}_u^R$ ($\mathbf{G}_g^I$ and $\mathbf{G}_u^I$) are the symmetric and antisymmetric components of the real (imaginary) part of the gradient vector $\mathbf{G}$. Equation 7 may be expressed in terms of a coupled set of linear equations for a real symmetric matrix

$$\begin{pmatrix} \mathbf{E}^{[2]} & -\omega\mathbf{S}^{[2]} & \gamma\mathbf{S}^{[2]} & 0 \\ -\omega\mathbf{S}^{[2]} & \mathbf{E}^{[2]} & 0 & \gamma\mathbf{S}^{[2]} \\ \gamma\mathbf{S}^{[2]} & 0 & -\mathbf{E}^{[2]} & \omega\mathbf{S}^{[2]} \\ 0 & \gamma\mathbf{S}^{[2]} & \omega\mathbf{S}^{[2]} & -\mathbf{E}^{[2]} \end{pmatrix} \begin{pmatrix} \mathbf{X}_g^R \\ \mathbf{X}_u^R \\ \mathbf{X}_u^I \\ \mathbf{X}_g^I \end{pmatrix} = \begin{pmatrix} \mathbf{G}_g^R \\ \mathbf{G}_u^R \\ -\mathbf{G}_u^I \\ -\mathbf{G}_g^I \end{pmatrix} \tag{10}$$

where the coupling between the different components is considered explicitly. Equation 10 may be solved in the reduced subspace spanned by real vectors

$$\mathbf{b}_g^p = \{\mathbf{b}_{1g}^R, \mathbf{b}_{1g}^I, \mathbf{b}_{2g}^R, \mathbf{b}_{2g}^I, ..., \mathbf{b}_{pg}^R, \mathbf{b}_{pg}^I\} \tag{11a}$$

$$\mathbf{b}_u^q = \{\mathbf{b}_{1u}^R, \mathbf{b}_{1u}^I, \mathbf{b}_{2u}^R, \mathbf{b}_{2u}^I, ..., \mathbf{b}_{qu}^R, \mathbf{b}_{qu}^I\} \tag{11b}$$

and the corresponding sets of linear transformations

$$\boldsymbol{\sigma}_g^p = \{\boldsymbol{\sigma}_{1g}^R, \boldsymbol{\sigma}_{1g}^I, \boldsymbol{\sigma}_{2g}^R, \boldsymbol{\sigma}_{2g}^I, ..., \boldsymbol{\sigma}_{ng}^R, \boldsymbol{\sigma}_{ng}^I\} \tag{12a}$$

$$\boldsymbol{\sigma}_u^q = \{\boldsymbol{\sigma}_{1u}^R, \boldsymbol{\sigma}_{1u}^I, \boldsymbol{\sigma}_{2u}^R, \boldsymbol{\sigma}_{2u}^I, ..., \boldsymbol{\sigma}_{nu}^R, \boldsymbol{\sigma}_{nu}^I\} \tag{12b}$$

where $p, q \leq 2n$, due to the orthonormalization condition. Equation 10 is solved in a reduced space of $\mathbf{b}_g^p$ and $\mathbf{b}_u^q$ in eq 3, giving a reduced space equation of the form

$$\begin{pmatrix} \mathbf{E}_{red,gg}^{[2]} & -\omega(\mathbf{S}_{red,ug}^{[2]})^T & \gamma(\mathbf{S}_{red,ug}^{[2]})^T & 0 \\ -\omega\mathbf{S}_{red,ug}^{[2]} & \mathbf{E}_{red,uu}^{[2]} & 0 & \gamma\mathbf{S}_{red,ug}^{[2]} \\ \gamma\mathbf{S}_{red,ug}^{[2]} & 0 & -\mathbf{E}_{red,uu}^{[2]} & \omega\mathbf{S}_{red,ug}^{[2]} \\ 0 & \gamma(\mathbf{S}_{red,ug}^{[2]})^T & \omega(\mathbf{S}_{red,ug}^{[2]})^T & -\mathbf{E}_{red,gg}^{[2]} \end{pmatrix} \begin{pmatrix} (\mathbf{X}_g^R)_{red} \\ (\mathbf{X}_u^R)_{red} \\ (\mathbf{X}_u^I)_{red} \\ (\mathbf{X}_g^I)_{red} \end{pmatrix} = \begin{pmatrix} (\mathbf{G}_g^R)_{red} \\ (\mathbf{G}_u^R)_{red} \\ -(\mathbf{G}_u^I)_{red} \\ -(\mathbf{G}_g^I)_{red} \end{pmatrix} \tag{13}$$

where

$$[(\mathbf{G}_g^R)_{red}]_i = (\mathbf{b}_g)_i^T \mathbf{G}_g^R, \; [(\mathbf{G}_u^R)_{red}]_i = (\mathbf{b}_u)_i^T \mathbf{G}_u^R$$

$$[(\mathbf{G}_u^I)_{red}]_i = (\mathbf{b}_u)_i^T \mathbf{G}_u^I, \; [(\mathbf{G}_g^I)_{red}]_i = (\mathbf{b}_g)_i^T \mathbf{G}_g^I$$

$$(\mathbf{E}_{red,gg}^{[2]})_{ij} = (\mathbf{b}_g)_i^T \mathbf{E}^{[2]} (\mathbf{b}_g)_j = (\mathbf{b}_g)_i^T (\boldsymbol{\sigma}_g)_j$$

$$(\mathbf{E}_{red,uu}^{[2]})_{ij} = (\mathbf{b}_u)_i^T \mathbf{E}^{[2]} (\mathbf{b}_u)_j = (\mathbf{b}_u)_i^T (\boldsymbol{\sigma}_u)_j$$

$$(\mathbf{S}_{red,ug}^{[2]})_{ij} = (\mathbf{b}_u)_i^T \mathbf{S}^{[2]} (\mathbf{b}_g)_j = (\mathbf{b}_u)_i^T (\boldsymbol{\rho}_u)_j \tag{14}$$

The optimal vectors in the subspace in eqs 11a and 11b are of the form

$$(\mathbf{X}_g^R)_{n+1} = \sum_{i=1}^{p} [(\mathbf{X}_g^R)_{red}]_i \mathbf{b}_{ig}; \quad (\mathbf{X}_u^R)_{n+1} = \sum_{i=1}^{q} [(\mathbf{X}_u^R)_{red}]_i \mathbf{b}_{iu} \tag{15a}$$

$$(\mathbf{X}_u^I)_{n+1} = \sum_{i=1}^{q} [(\mathbf{X}_u^I)_{red}]_i \mathbf{b}_{iu}; \quad (\mathbf{X}_g^I)_{n+1} = \sum_{i=1}^{p} [(\mathbf{X}_g^I)_{red}]_i \mathbf{b}_{ig} \tag{15b}$$

The residual calculated to check for convergence is given as

$$\mathbf{R} = \mathbf{R}^R + i\mathbf{R}^I = \mathbf{R}_g^R + \mathbf{R}_u^R + i(\mathbf{R}_g^I + \mathbf{R}_u^I) \tag{16}$$

where

$$\mathbf{R}_g^R = \mathbf{E}^{[2]}\mathbf{X}_g^R - \omega\mathbf{S}^{[2]}\mathbf{X}_u^R + \gamma\mathbf{S}^{[2]}\mathbf{X}_u^I - \mathbf{G}_g^R$$

$$\mathbf{R}_u^R = \mathbf{E}^{[2]}\mathbf{X}_u^R - \omega\mathbf{S}^{[2]}\mathbf{X}_g^R + \gamma\mathbf{S}^{[2]}\mathbf{X}_g^I - \mathbf{G}_u^R$$

$$\mathbf{R}_u^I = -\mathbf{E}^{[2]}\mathbf{X}_u^I + \omega\mathbf{S}^{[2]}\mathbf{X}_g^I + \gamma\mathbf{S}^{[2]}\mathbf{X}_g^R + \mathbf{G}_u^I$$

$$\mathbf{R}_g^I = -\mathbf{E}^{[2]}\mathbf{X}_g^I + \omega\mathbf{S}^{[2]}\mathbf{X}_u^I + \gamma\mathbf{S}^{[2]}\mathbf{X}_u^R + \mathbf{G}_g^I \tag{17}$$

In the subspace iterative approach, new trial vectors are obtained by preconditioning residuals

$$\begin{pmatrix} \mathbf{b}_{n+1,g}^R \\ \mathbf{b}_{n+1,u}^R \\ \mathbf{b}_{n+1,u}^I \\ \mathbf{b}_{n+1,g}^I \end{pmatrix} = \mathcal{P} \otimes \begin{pmatrix} \mathcal{A} & \mathcal{B} & C & \mathcal{D} \\ \mathcal{B} & \mathcal{A} & \mathcal{D} & C \\ C & \mathcal{D} & -\mathcal{A} & -\mathcal{B} \\ \mathcal{D} & C & -\mathcal{B} & -\mathcal{A} \end{pmatrix} \begin{pmatrix} \mathbf{R}_g^R \\ \mathbf{R}_u^R \\ \mathbf{R}_u^I \\ \mathbf{R}_g^I \end{pmatrix} \tag{18}$$

where $\mathcal{P}$, $\mathcal{A}$, $\mathcal{B}$, C and $\mathcal{D}$ are given by

$$\mathcal{P} = \{[(\mathbf{E}_0^{[2]})^2 - (\omega^2 - \gamma^2)(\mathbf{S}_0^{[2]})^2]^2 + 4\omega^2\gamma^2(\mathbf{S}_0^{[2]})^4\}^{-1}$$

$$\mathcal{A} = \mathbf{E}_0^{[2]}[(\mathbf{E}_0^{[2]})^2 - (\omega^2 - \gamma^2)(\mathbf{S}_0^{[2]})^2]$$

$$\mathcal{B} = \omega\mathbf{S}_0^{[2]}[(\mathbf{E}_0^{[2]})^2 - (\omega^2 + \gamma^2)(\mathbf{S}_0^{[2]})^2]$$

$$C = \gamma\mathbf{S}_0^{[2]}[(\mathbf{E}_0^{[2]})^2 + (\omega^2 + \gamma^2)(\mathbf{S}_0^{[2]})^2]$$

$$\mathcal{D} = 2\omega\gamma\mathbf{E}_0^{[2]}(\mathbf{S}_0^{[2]})^2 \tag{19}$$

$\mathbf{E}_0^{[2]}$ and $\mathbf{S}_0^{[2]}$ are diagonal approximations to $\mathbf{E}^{[2]}$ and $\mathbf{S}^{[2]}$, respectively. In the single determinant HF or KS-DFT approximations, in the molecular orbital basis $\mathbf{E}_0^{[2]}$ contains the difference between virtual and occupied orbital energies and $(\mathbf{S}_0^{[2]})^2 = \mathbf{1}$. The condition number of eq 10 is significantly reduced by the preconditioning in eq 18, which leads to a significant reduction in the number of iterations needed to obtain convergence.

New trial vectors obtained in eq 18 are orthogonalized against the corresponding sets of vectors in eq 11, using the Gram-Schmidt orthogonalization technique. Then, if not below a given threshold, the trial vectors are normalized and linear transformations $\mathbf{E}^{[2]}\mathbf{b}_{n+1}$ are performed. The new trial vectors and linear transformations are added to the corresponding subspaces in eqs 11 and 12, respectively. The iterative sequence is continued until convergence is obtained, i.e. until the norm of the residual is smaller than a preset threshold.

The most computationally demanding step in the algorithm is performing linear transformations $\boldsymbol{\sigma} = \mathbf{E}^{[2]}\mathbf{b}$ in eq 8a. The computational cost of obtaining a linear transformation of a symmetric or an antisymmetric vector is a half comparing to a general vector of the same size. Thus, in the implementation in Dalton2013, the linear transformations are performed on a sum of $\mathbf{b}_{i,g}$ and $\mathbf{b}_{i,u}$ and we count one linear transformation for this

dx.doi.org/10.1021/ct500114m | J. Chem. Theory Comput. 2014, 10, 2449−2455

pair. Therefore, in each iteration two linear transformations are required on a real and imaginary vector **b**. To obtain linear transformation $\boldsymbol{\sigma}_i$, a perturbed Fock matrix must be calculated from a density matrix. This process is memory-wise very expensive, since two-electron integrals are required. Due to the complexity and dimension of biological systems of interest, the integrals cannot be stored in memory but must be calculated in every iteration, which is the most computationally expensive step of the procedure. However, since the integrals are independent of the density matrix, within one iteration they can be used in calculation of several Fock matrices. Thus, it may be beneficial to solve eq 6 for several frequencies simultaneously. This way, more vectors are added to the reduced space in eq 11 in each iteration, faster spanning a larger space that, in consequence, reduces the number of iteration needed to obtain convergence. On top of it, in Dalton2013, the process of obtaining linear transformations is parallelized and several Fock matrices can be constructed without an additional cost comparing to a single one. Therefore, the cost of the calculation does not scale with the total number of Fock matrices constructed. In practice, since in the calculation of molecular spectra eq 6 is solved for many close lying frequencies, there is a high linear dependence between vectors and it is highly beneficial to solve them simultaneously, as will be shown in the next section.

IV. RESULTS AND DISCUSSION

The structure of the C_{60} fullerene has been optimized with the Gaussian03 program,[50] at the DFT level with the hybrid B3LYP exchange-correlation functional[51,52] employing the correlation-consistent, polarized valence, double-ζ (cc-pVDZ) basis set of Dunning.[53] The calculations of the polarizability have been performed with the Dalton2013 program[49] using the CPP solver employing the algorithm with symmetrized trial vectors,[11] described in details in section III. C_{2h} symmetry has been adopted in the calculation. The hybrid B3LYP functional have been used in the calculations of the spectra in both the UV−vis and X-ray regions. Although X-ray absorption spectra are strongly dependent on the choice of exchange-correlation functional, we have chosen to adopt a common functional in the present work. We motivate this choice by the fact that our predominant interest is to display the performance of the proposed algorithm. The polarization basis set of Sadlej[54] that is optimized with respect to the atomic static polarizability has been used in all property calculation and it is a sufficiently flexible and diffuse basis set to challenge the numerical stability of our algorithm. For carbon the basis set contraction is [10*s*6*p*4*d*|5*s*3*p*2*d*] and spherical basis functions have been employed. Thus, the overall number of basis functions is 1440. The relaxation parameter that govern the broadening of the absorption spectra has been chosen as γ = 1000 cm^{-1} and damped response equations have been solved to a relative residual norm of 10^{-4}. The UV−vis and X-ray absorption spectra are given in atomic units.

In Figure 1, the spectrum of fullerene C_{60} in the UV−vis region has been presented. The lowest electronic states in C_{60} correspond to electric-dipole forbidden transitions of *gerade* symmetry. The lowest singlet states (found at around 1.9 eV) showed to be nearly degenerate and of T_{1g}, T_{2g}, and G_g symmetry.[55] The first electric-dipole allowed states of symmetry T_{1u} are found at higher energies. The experimental study[56] shows three main peaks at energies of 3.6, 4.6, and 5.6 eV with spectral shoulders noticed at 2.8 and 6.4 eV. The spectrum depicted in Figure 1 is in an excellent agreement with the experimental

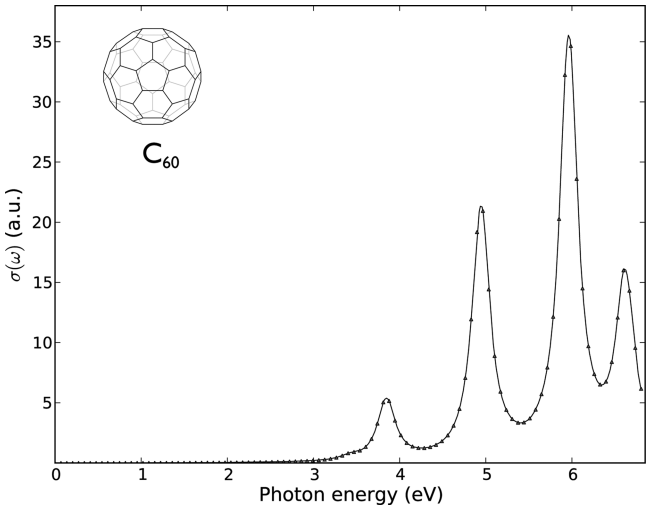

Figure 1. (Color online) UV−vis absorption spectrum of C_{60} fullerene as obtained at the KS-DFT/B3LYP level of theory.

results. The first strong signal is due to a single state, namely 1^1T_{1u}, whereas the next two peaks are due to two signals associated with states 2^1T_{1u} and 3^1T_{1u}.

Figure 2 illustrates the convergence characteristics of the CPP algorithm at six representative frequency values, namely: 0.0,

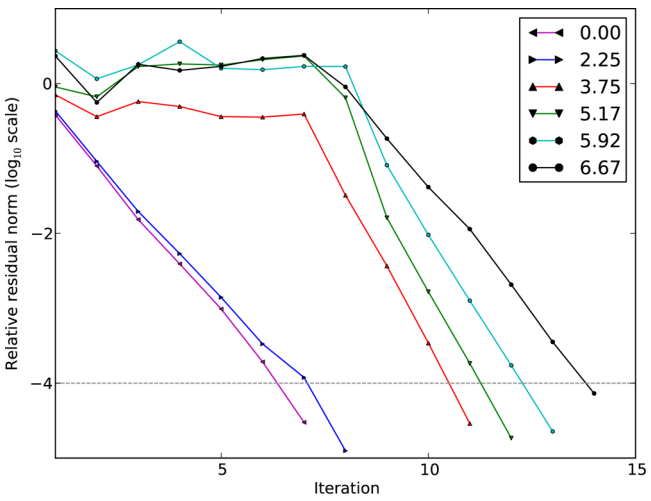

Figure 2. (Color online) Relative residual norm versus iteration number for the linear response equation at a selection of frequencies (see legend) in the UV−vis region (0.0−6.8 eV). All 101 equations have been solved simultaneously. Calculations have been performed for the C_{60} fullerene at the KS-DFT/B3LYP level of theory using the polarization basis set of Sadlej and a damping term γ = 1000 cm^{-1}.

2.25, 3.75, 5.17, 5.92, and 6.67 eV. To obtain a spectral resolution of the entire region 0−6.8 eV, eq 6 needs to be solved for some 100 equidistant frequencies. The damping factor γ = 1000 cm^{-1} (0.0045566 au, 0.12 eV), as a half width at half-maximum of a peak, determines a required resolution of the spectrum. In this work, a step of ≈0.07 eV (0.0025 au) has been adopted. The calculation has been performed for 101 frequencies in the region: from 0.0 to 6.8 eV, giving 101 equations that have been solved simultaneously. Rapid convergence (in 7 and 8 iterations) has been observed for all equations in the off-resonance frequencies (0.0 and 2.25 eV). At resonance frequencies, convergence is expected to be the slowest and yet only 14 iterations are required

to obtain the solution vector at ω = 6.67 eV. As can be seen in Figure 2, the norm of the residual shows a plateau in the first few iterations for resonance frequencies. It is due to the fact that in proximity of a resonance, the preconditioner is close to being singular and therefore the initial trial vectors (i.e., the preconditioned property gradient vector) are poor (see ref 11 for a detailed discussion). A few (8 for ω = 6.67 eV) iterations are required to obtained a reasonable optimal solution vector that then monotonically converges in next 6 iterations.

In Figure 3, a total number of solved equations (bars) is compared with a total number of linear transformations

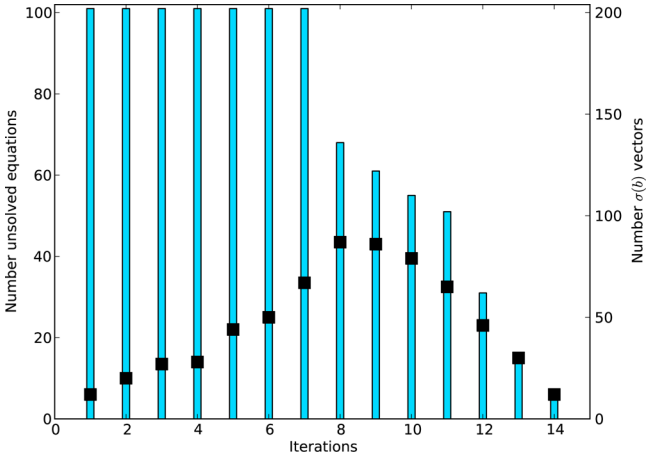

Figure 3. (Color online) Total number of solved equations (bars) compared with the total number of linear transformations (squares) performed in every iteration for a calculation of the UV−vis spectrum (0.0−6.8 eV). All 101 equations have been solved simultaneously to a relative residual threshold of 10^{-4}. Calculations have been performed for the C_{60} fullerene at the KS-DFT/B3LYP level of theory using the polarization basis set of Sadlej and a damping term γ = 1000 cm^{-1}.

(squares) performed in every iteration for a calculation of the UV−vis spectrum presented in Figure 1. All 101 equations have been solved simultaneously in a frequency region between 0.0 and 6.8 eV. When eq 6 is solved for a single frequency, then, in each iteration, two linear transformations $\mathbf{E}^{[2]}\mathbf{b}$ are performed, as discussed in the previous section. When more equations are solved simultaneously, the number of linear transformations is equal or less than the twice the number of solved equations, due to an orthogonalization condition. It can be seen in Figure 3 that when all 101 frequencies are addressed, this number is strongly reduced. In the first iterations, there is a large linear dependence between trial vectors and less than 40 linear transformations need to be performed in every iteration to converge over 30 damped response equations (in 8 iterations). In the following iterations, less linear dependence among trial vectors is observed and higher number of linear transformations need to be calculated. However, it should be noted that the number has not exceeded 90. When the convergence has been obtained for over half of the equations, the number of linear transformation starts decreasing. In iteration 13, when 15 equations remain unsolved, all trial vectors are linearly independent and this trend follows until the last equation reaches convergence. The process of obtaining linear transformations is parallelized; therefore, several linear transformations are performed without an additional cost comparing to a single one.

In Figure 4, the near-edge X-ray absorption fine structure (NEXAFS) spectrum of fullerene C_{60} has been presented, where

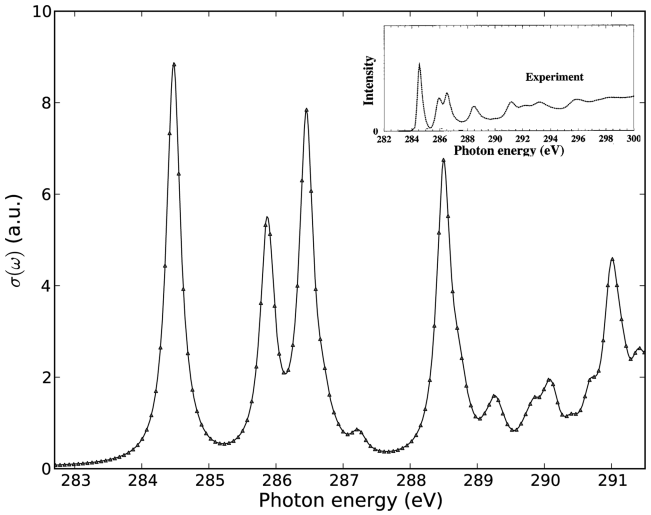

Figure 4. (Color online) NEXAFS spectrum of the C_{60} fullerene as obtained at the KS-DFT/B3LYP level of theory. Experimental data are taken from ref 57.

the experimental data are taken from ref 57. The experimental NEXAFS spectrum of C_{60} has four discrete levels before the continuum.[57,58] The first three peaks can be assigned as electronic transitions to the virtual orbitals of symmetry t_{1u}, t_{1g}, t_{2u}, and h_g, where the latter two are energetically near degenerate. The fourth absorption band corresponds to the unoccupied orbitals with symmetries h_u, t_{1u}, a_g, and g_g.[57] The general structure of calculated spectrum is, within the adopted approximation, in a very good agreement with the experimental results. Due to the nature of standard KS-DFT, there is a need to apply an overall spectral shift of 10.6 eV to account for the inherent self-interaction error.[24]

In Figure 5, the convergence of the damped response equation at the near-resonance frequency ω = 286.46 eV is presented, as 1, 5, 21, 51, and 131 equations have been solved simultaneously. In Table 1, we report the total number of iterations, size of the

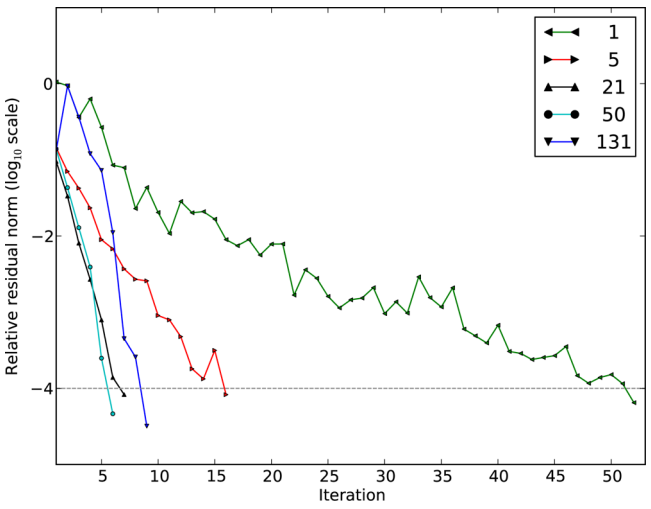

Figure 5. (Color online) Relative residual norm versus iteration number for the response equation at the near-resonance frequency ω = 286.46 eV, as 1, 5, 21, 51, and 131 equations have been solved simultaneously. Calculations have been performed for the C_{60} fullerene at the KS-DFT/B3LYP level of theory using the polarization basis set of Sadlej and a damping term γ = 1000 cm^{-1}.

dx.doi.org/10.1021/ct500114m | J. Chem. Theory Comput. 2014, 10, 2449−2455

Table 1. Convergence Details for the Solution of the Damped Response Equations, as 1, 5, 21, 51, and 131 Equation Have Been Solved Simultaneously to a Relative Residual Threshold of 10^{-4}[a]

N_ω	$N_{it}^{286.46}$	N_{it}^{tot}	N_g^{red}	N_u^{red}	N_σ^{tot}
1	52	52	104	104	104
5	16	17	154	154	154
21	7	14	280	280	280
51	6	7	472	472	472
131	9	28	2097	2096	2097

[a]Number of solved equation (first column); number of iterations to converge the equation for ω = 286.46 eV (second column); the total number of iterations to converge all equations in a chosen interval (third column); total size of the reduced spaces $\mathbf{b}_g$ and $\mathbf{b}_u$ in eq 11 (fourth and fifth columns); total number of Fock matrices needed to be constructed during the iterative procedure while solving eq 6 in the chosen interval of frequencies (sixth).

reduce spaces (eqs 11) and linear transformations, in calculations presented in Figure 5. In the second and third column, the number of iterations needed to converge the chosen frequency (ω = 286.46 eV) and all the equations in the chosen interval (the first column) is given, respectively. The total size of the reduced spaces $\boldsymbol{b}_g$ and $\boldsymbol{b}_u$ in eq 11 are reported in the fourth and fifth column. In the sixth column, we present the total number of Fock matrices that need to be constructed during the iterative procedure while solving eq 6 in a chosen interval of frequencies. As can be seen in Figure 5, convergence is the slowest, when eq 6 is solved for a single frequency; 52 iterations are then required to obtain convergence. When 5 and 21 equations are solved simultaneously, convergence for ω = 286.46 eV is obtained in 16 and 7 iterations, respectively. Only 17 and 14 iterations are required to converge all equations in the frequency ranges 286.32−286.59 and 285.78−287.14 eV, respectively. The whole spectrum of interest (282.71−291.56 eV) converged in only 28 iterations, by solving a set of 131 equations. Convergence for ω = 286.46 eV has then been obtained in 9 iterations. Based on the results presented in Figure 5, it can be concluded that it is highly advantageous to solve damped response equations for more than one frequency at a time. By solving eq 6 in a larger reduced space obtained by solving for several frequencies of interest, it is not only that more solutions are calculated without an additional cost, but the computational time decreases as the number of iterations becomes smaller.

V. CONCLUSIONS

We have investigated the performance of an algorithm for solving damped linear response equations with focus on the spectral resolution of a window of frequencies. With the complex polarization propagator approach, the UV−vis and pre-edge X-ray absorption spectra of the C_{60} fullerene has been determined at the KS-DFT level of theory in conjunction with the standard B3LYP functional and a flexible triple-ζ basis set with diffuse functions. It is demonstrated that the linear response equation solver is numerically very stable providing smooth convergence also in resonance regions of the spectrum and allowing for a very tight convergence criterion. In addition to stability, the linear response equation solver also demonstrates superb efficiency. The entire UV−vis and X-ray spectral regions converge to a relative residual norm of 10^{-4} in 14 and 28 iterations, respectively, and the separate regions span 6.8 and 8.8 eV and require the solution of 101 and 131 linear response equations in order to obtain the requested high-resolution spectra. In fact, the calculations of the complete spectra are made at a lower computational effort as compared to the corresponding single frequency calculations—the convergence of the linear response equation for a single frequency of 286.46 eV requires more than 50 iterations.

The algorithm has been implemented in the MO-based module of the Dalton program and is distributed with the 2013 release version of the program.[49] The algorithm as such, however, is not limited to an MO formulation of response theory and it will also be implemented in the atomic-orbital driven part of Dalton (LSDalton) that displays linear scaling characteristics.

AUTHOR INFORMATION

Corresponding Authors

*Email: joaka@ifm.liu.se.

*Email: panor@ifm.liu.se.

Notes

The authors declare no competing financial interest.

ACKNOWLEDGMENTS

P.N. acknowledges financial support from the Swedish Research Council (Grant No. 621-2010-5014). The authors acknowledge a grant for computing time from National Supercomputer Centre (NSC), Sweden.

REFERENCES

(1) Olsen, J.; Jørgensen, P. *J. Chem. Phys.* **1985**, *82*, 3235−3264.

(2) Bai, Z.; Demmel, J.; Dongarra, J.; Ruhe, A.; van der Vorst, H. *Templates for the Solution of Algebraic Eigenvalue Problems. A Practical Guide*; SIAM: Philadelphia, 2000; pp 56−63.

(3) Coriani, S.; Christiansen, O.; Fransson, T.; Norman, P. *Phys. Rev. A* **2012**, *85*, 022507(8). Coriani, S.; Fransson, T.; Christiansen, O.; Norman, P. *J. Chem. Theory Comput.* **2012**, *8* (5), 1616−1628.

(4) Fransson, T.; Coriani, S.; Christiansen, O.; Norman, P. *J. Chem. Phys.* **2013**, *138*, 124311(12).

(5) Norman, P.; Bishop, D. M.; Jensen, H. J. A.; Oddershede, J. *J. Chem. Phys.* **2001**, *115*, 10323−10334.

(6) Norman, P.; Bishop, D. M.; Jensen, H. J. A.; Oddershede, J. *J. Chem. Phys.* **2005**, *123*, 194103(18).

(7) Norman, P. *Phys. Chem. Chem. Phys.* **2011**, *13*, 20519−20535.

(8) Orr, B. J.; Ward, J. F. *Mol. Phys.* **1971**, *20*, 513−526.

(9) Barron, L. *Molecular Light Scattering and Optical Activity*, 2nd ed.; Cambridge University Press: Cambridge, U.K., 2004; pp 94−103.

(10) Kristensen, K.; Kauczor, J.; Kjærgaard, T.; Jørgensen, P. *J. Chem. Phys.* **2009**, *131*, 044112(33).

(11) Kauczor, J.; Jørgensen, P.; Norman, P. *J. Chem. Theory Comput.* **2011**, *7*, 1610−1630.

(12) Boyd, R. W. *Nonlinear Optics*, 3 ed.; Academic Press: New York, 2008; pp 155−157.

(13) Sakurai, J. J. *Modern Quantum Mechanics*; Addison-Wesley: Boston, 1994; pp 341−345.

(14) Norman, P.; Jiemchooroj, A.; Sernelius, B. E. *J. Chem. Phys.* **2003**, *118*, 9167−9174. Norman, P.; Jiemchooroj, A.; Sernelius, B. E. *J. Comput. Methods Sci. Eng.* **2004**, *4*, 321−332. Jiemchooroj, A.; Norman, P.; Sernelius, B. E. *J. Chem. Phys.* **2005**, *123*, 124312(6). Jiemchooroj, A.; Norman, P.; Sernelius, B. E. *J. Chem. Phys.* **2006**, *125*, 124306(5).

(15) Blase, X.; Ordejón, P. *Phys. Rev. B* **2004**, *69*, 085111(10).

(16) Jensen, L.; Autschbach, J.; Schatz, G. C. *J. Chem. Phys.* **2005**, *122*, 224115(11).

(17) Devarajan, A.; Gaenko, A.; Autschbach, J. *J. Chem. Phys.* **2009**, *130*, 194102(13).

(18) Mata, R. A.; Cabral, B. J. C.; Millot, C.; Coutinho, K.; Canuto, S. *J. Chem. Phys.* **2009**, *130*, 014505(8).

(19) Kauczor, J.; Norman, P.; Saidi, W. A. *J. Chem. Phys.* **2013**, *138*, 114107(8).
(20) Norman, P.; Ruud, K.; Helgaker, T. *J. Chem. Phys.* **2004**, *120*, 5027−5035.
(21) Jiemchooroj, A.; Norman, P. *J. Chem. Phys.* **2007**, *126*, 134102(7).
(22) Autschbach, J.; Jensen, L.; Schatz, G. C.; Tse, Y. C. E.; Krykunov, M. *J. Phys. Chem. A* **2006**, *110*, 2461−2473. Krykunov, M.; Autschbach, J. *J. Chem. Phys.* **2006**, *125*, 034102(10). Krykunov, M.; Kundrat, M. D.; Autschbach, J. *J. Chem. Phys.* **2006**, *125*, 194110(13).
(23) Ekström, U.; Norman, P.; Carravetta, V.; Ågren, H. *Phys. Rev. Lett.* **2006**, *97*, 143001(4). Ekström, U.; Norman, P. *Phys. Rev. A* **2006**, *74*, 042722(7).
(24) Tu, G.; Rinkevicius, Z.; Vahtras, O.; Ågren, H.; Ekström, U.; Norman, P.; Carravetta, V. *Phys. Rev. A* **2007**, *76*, 022506(7).
(25) Jiemchooroj, A.; Ekström, U.; Norman, P. *J. Chem. Phys.* **2007**, *127*, 165104(8). Jiemchooroj, A.; Norman, P. *J. Chem. Phys.* **2008**, *128*, 234304(4).
(26) Linares, M.; Stafström, S.; Norman, P. *J. Chem. Phys.* **2009**, *130*, 104305(7). Linares, M.; Stafström, S.; Rinkevicius, Z.; Ågren, H.; Norman, P. *J. Phys. Chem. B* **2011**, *115*, 5096−5102.
(27) Ahrén, M.; Selegård, L.; Söderlind, F.; Linares, M.; Kauczor, J.; Norman, P.; Käll, P.-O.; Uvdal, K. *J. Nanopart. Res.* **2012**, *14*, 1006(17).
(28) Krykunov, M.; Autschbach, J. *J. Chem. Phys.* **2007**, *126*, 024101(12).
(29) Jensen, L.; Zhao, L. L.; Autschbach, J.; Schatz, G. C. *J. Chem. Phys.* **2005**, *123*, 174110(11).
(30) Zhao, L. L.; Jensen, L.; Schatz, G. C. *Nano Lett.* **2006**, *6*, 1229−1234. Zhao, L. L.; Jensen, L.; Schatz, G. C. *J. Am. Chem. Soc.* **2006**, *128*, 2911−2919. Zhao, L. L.; Schatz, G. C. *J. Phys. Chem. A* **2006**, *110*, 5973−5977.
(31) Aikens, C. M.; Schatz, G. C. *J. Phys. Chem. A* **2006**, *110*, 13317−13324.
(32) Jensen, L.; Autschbach, J.; Krykunov, M.; Schatz, G. C. *J. Chem. Phys.* **2007**, *127*, 134101(11). Jensen, L.; Zhao, L. L.; Schatz, G. C. *J. Phys. Chem. C* **2007**, *111*, 4756−4764. Jensen, L.; Aikens, C. M.; Schatz, G. C. *Chem. Soc. Rev.* **2008**, *37*, 1061−1073.
(33) Zheng, Y. B.; Yang, Y.-W.; Jensen, L.; Fang, L.; Juluri, B. K.; Flood, A. H.; Weiss, P. S.; Stoddart, J. F.; Huang, T. J. *Nano Lett.* **2009**, *9*, 819−825.
(34) Mohammed, A.; Ågren, H.; Norman, P. *Chem. Phys. Lett.* **2009**, *468*, 119−123. Mohammed, A.; Ågren, H.; Norman, P. *Phys. Chem. Chem. Phys.* **2009**, *11*, 4539−4548.
(35) Al-Saidi, W. A.; Asher, S. A.; Norman, P. *J. Phys. Chem. A* **2012**, *116*, 7862−7872. Saidi, W. A.; Norman, P. *Phys. Chem. Chem. Phys.* **2014**, *16*, 1479−1486. Saidi, W. A.; Norman, P. *Carbon* **2014**, *67*, 17−26.
(36) Krykunov, M.; Seth, M.; Ziegler, T.; Autschbach, J. *J. Chem. Phys.* **2007**, *127*, 244102(16).
(37) Solheim, H.; Ruud, K.; Coriani, S.; Norman, P. *J. Chem. Phys.* **2008**, *128*, 094103(7). Solheim, H.; Ruud, K.; Coriani, S.; Norman, P. *J. Phys. Chem. A* **2008**, *112*, 9615−9618.
(38) Kjærgaard, T.; Kristensen, K.; Kauczor, J.; Jørgensen, P.; Coriani, S.; Thorvaldsen, A. J. *J. Chem. Phys.* **2011**, *135*, 024112(16).
(39) Fahleson, T.; Kauczor, J.; Norman, P.; Coriani, S. *Mol. Phys.* **2013**, *111*, 1401−1404.
(40) Kristensen, K.; Kauczor, J.; Thorvaldsen, A. J.; Jørgensen, P.; Kjærgaard, T.; Rizzo, A. *J. Chem. Phys.* **2011**, *134*, 024104(17).
(41) Milne, B. F.; Norman, P.; Nogueira, F.; Cardoso, C. *Phys. Chem. Chem. Phys.* **2013**, *15*, 14814−14822.
(42) Olsen, J.; Jensen, H. J. A.; Jørgensen, P. *J. Comput. Phys.* **1988**, *74*, 265−282.
(43) Davidson, E. R. *J. Comput. Phys.* **1975**, *17*, 87−94.
(44) Saue, T. In *Relativistic Electronic Structure Theory. Part 1: Fundamentals*; Schwerdtfeger, P., Ed.; Elsevier: Amsterdam, 2002; Chapter 7, pp 332−400; Saue, T.; Jensen, H. J. A. *J. Chem. Phys.* **2003**, *118*, 522−536.
(45) Bast, R.; Jensen, H. J. A.; Saue, T. *Int. J. Quantum Chem.* **2009**, *109*, 2091−2112.
(46) Villaume, S.; Saue, T.; Norman, P. *J. Chem. Phys.* **2010**, *133*, 064105(10).
(47) Pedersen, M. N.; Hedegård, E. D.; Olsen, J. M. H.; Kauczor, J.; Norman, P.; Kongsted, J. *J. Chem. Theory Comput.* **2014**, *10*, 1164−1171.
(48) Kauczor, J.; Norman, P.; Christiansen, O.; Coriani, S. *J. Chem. Phys.* **2013**, *139*, 211102(4).
(49) DALTON, a molecular electronic structure program, release Dalton2013. Aidas, K.; Angeli, C.; Bak, K.; Bakken, V.; Boman, L.; Bast, R.; Christiansen, O.; Cimiraglia, R.; Coriani, S.; Dahle, P.; Dalskov, E.; Elkström, U.; Enevoldsen, T.; Eriksen, J. J.; Ettenhuber, P.; Fernandez, B.; Ferrighi, L.; Fliegl, H.; Frediani, L.; Hald, K.; Halkier, A.; Hättig, C.; Heiberg, H.; Helgaker, T.; Hennum, A.; Hettema, H.; Hjertenæs, E.; Høst, S.; Høyvik, I.-M.; Iozzi, M. F.; Jansik, B.; Jensen, H.J.Aa.; Jonsson, D.; Jørgensen, P.; Kauczor, J.; Kirpekar, S.; Kjærgaard, T.; Klopper, W.; Knecht, S.; Kobayashi, R.; Koch, H.; Kongsted, J.; Krapp, A.; Kristensen, K.; Ligabue, A.; Lutnæs, O. B.; Melo, J. I.; Mikkelsen, K. V.; Myhre, R. H.; Neiss, C.; Nielsen, C. B.; Norman, P.; Olsen, J.; Olsen, J. M. H.; Osted, A.; Packer, M. J.; Pawlowski, F.; Pedersen, T. B.; Provasi, P. F.; Reine, S.; Rinkevicius, Z.; Ruden, T. A.; Ruud, K.; Rybkin, V.; Salek, P.; Samson, C. C. M.; Sanchez de Meras, A.; Saue, T.; Sauer, S. P. A.; Schimmelpfennig, B.; Sneskov, K.; Steindal, A. H.; Sylvester-Hvid, K. O.; Taylor, P. R.; Teale, A. M.; Tellgren, E. I.; Tew, D. P.; Thorvaldsen, A. J.; Thøgersen, L.; Vahtras, O.; Watson, M. A.; Wilson, D. J. D.; Ziolkowski, M.; Ågren, H. *WIREs Comput. Mol. Sci.* **2014**, *4*, 269−284.
(50) Frisch, M. J.; Trucks, G. W.; Schlegel, H. B.; Scuseria, G. E.; Robb, M. A.; Cheeseman, J. R.; Montgomery, Jr., J. A. a. V.; Kudin, K. N.; Burant, J. C.; Millam, J. M.; Iyengar, S. S.; Tomasi, J.; Barone, V.; Mennucci, B.; Cossi, M.; Scalmani, G.; Rega, N.; Petersson, G. A.; Nakatsuji, H.; Hada, M.; Ehara, M.; Toyota, K.; Fukuda, R.; Hasegawa, J.; Ishida, M.; Nakajima, T.; Honda, Y.; Kitao, O.; Nakai, H.; Klene, M.; Li, X.; Knox, J. E.; Hratchian, H. P.; Cross, J. B.; Bakken, V.; Adamo, C.; Jaramillo, J.; Gomperts, R.; Stratmann, R. E.; Yazyev, O.; Austin, A. J.; Cammi, R.; Pomelli, C.; Ochterski, J. W.; Ayala, P. Y.; Morokuma, K.; Voth, G. A.; Salvador, P.; Dannenberg, J. J.; Zakrzewski, V. G.; Dapprich, S.; Daniels, A. D.; Strain, M. C.; Farkas, O.; Malick, D. K.; Rabuck, A. D.; Raghavachari, K.; Foresman, J. B.; Ortiz, J. V.; Cui, Q.; Baboul, A. G.; Clifford, S.; Cioslowski, J.; Stefanov, B. B.; Liu, G.; Liashenko, A.; Piskorz, P.; Komaromi, I.; Martin, R. L.; Fox, D. J.; Keith, T.; Al-Laham, M. A.; Peng, C. Y.; Nanayakkara, A.; Challacombe, M.; Gill, P. M. W.; Johnson, B.; Chen, W.; Wong, M. W.; Gonzalez, C.; Pople, J. A. *Gaussian 03*, RevisionE.01; Gausian, Inc.: Wallingford, CT, 2003.
(51) Becke, A. D. *J. Chem. Phys.* **1993**, *98*, 5648−5652.
(52) Stephens, P. J.; Devlin, F. J.; Chabalowski, C. F.; Frisch, M. J. *J. Phys. Chem.* **1994**, *98*, 11623−11627.
(53) Dunning, T. H. *J. Chem. Phys.* **1989**, *90*, 1007−1023.
(54) Sadlej, A. J. *Collect. Czech. Chem. Commun.* **1988**, *53*, 1995−2016.
(55) Sassara, A.; Zerza, G.; Chergui, M.; Negri, F.; Orlandi, G. *J. Chem. Phys.* **1997**, *107*, 8731−8741.
(56) Yagi, H.; Nakajima, K.; Koswattage, K. R.; Nakagawa, K.; Huang, C.; Prodhan, M. S. I.; Kafle, B. P.; Katayanagi, H.; Mitsuke, K. *Carbon* **2009**, *47* (4), 1152−1157.
(57) Luo, Y.; Ågren, H.; Gel'mukhanov, F. K.; Guo, J. H.; Skytt, P.; Wassdahl, N.; Nordgren, J. *Phys. Rev. B* **1995**, *52*, 14479−14496. Nyberg, M.; Luo, Y.; Triguero, L.; Pettersson, L. G. M.; Ågren, H. *Phys. Rev. B* **1999**, *60*, 7956−7960.
(58) Terminello, L. J.; Shuh, D. K.; Himpsel, F. J.; Lapiano-Smith, D. A.; Stör, J.; Bethune, D. S.; G, M. *Chem. Phys. Lett.* **1991**, *182*, 491−496.